Supporting Information

Molecular Level Design of Nitrogen–Doped Well–Defined Microporous Carbon Spheres for Selective Adsorption and Electrocatalysis

Zirun Chen, Shaohong Liu, Junlong Huang, Wen Huang, Luyi Chen, Yin Cui, Yang Du, and Ruowen Fu*

a. PCFM Lab, School of Chemistry, Sun Yat–sen University, Guangzhou 510275, China.
Email: cesfrw@mail.sysu.edu.cn

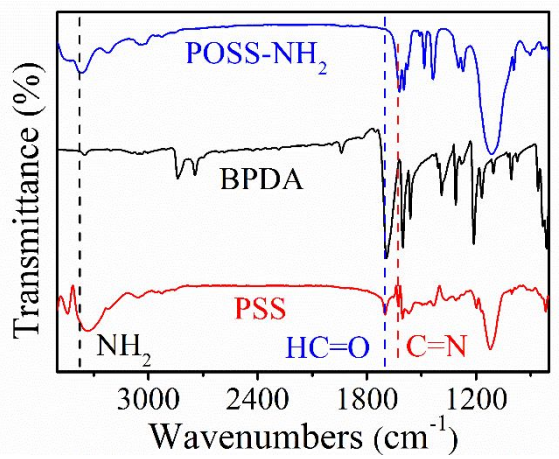

Figure S1. FT-IR spectra of PSS.

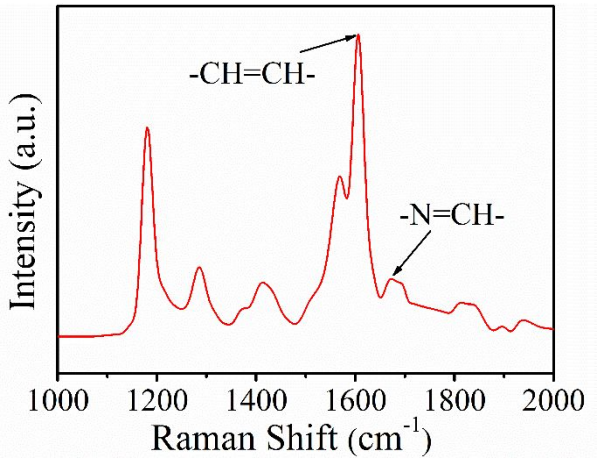

Figure S2. Raman spectra of PSS.

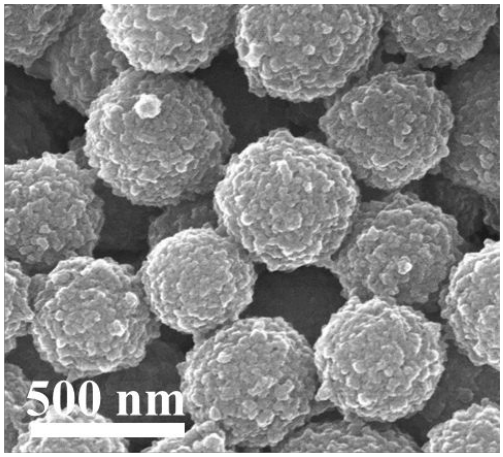

Figure S3. SEM image of PSS.

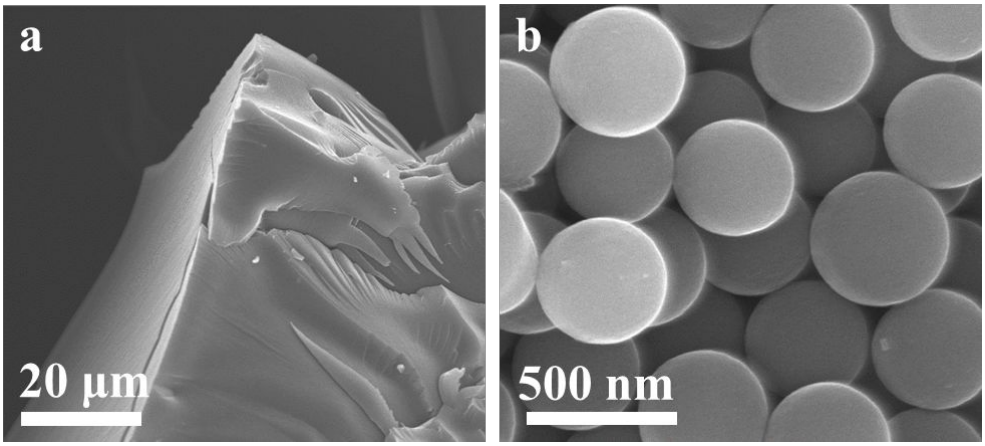

Figure S4. SEM images of (a) polymer particles and (b) polymer spheres.

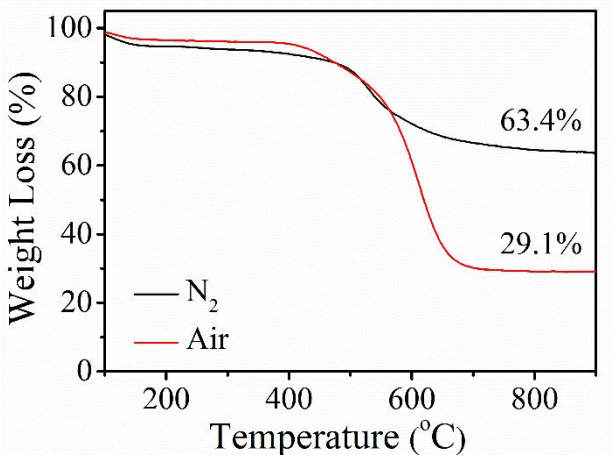

Figure S5. TGA curves of PSS.

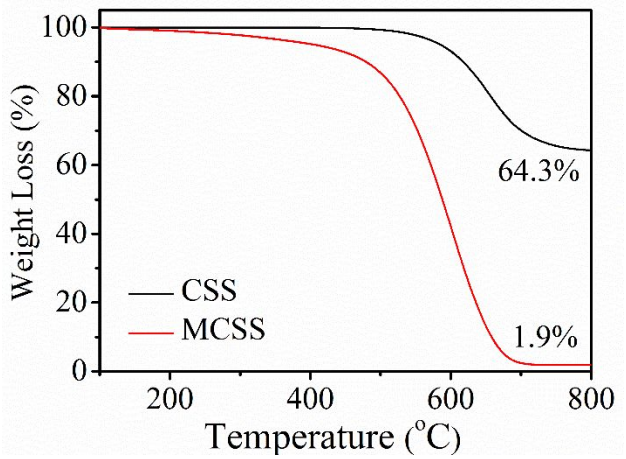

Figure S6. TGA curves of CSS and MCSS.

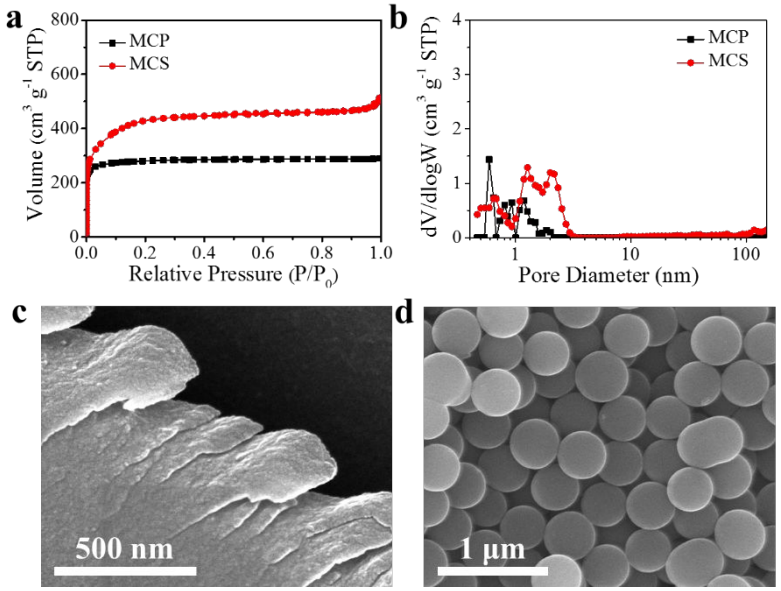

Figure S7. (a, b) N_2 adsorption-desorption isotherms and Pore size distribution of MCP and MCS. SEM images of (c) MCP and (d) MCS.

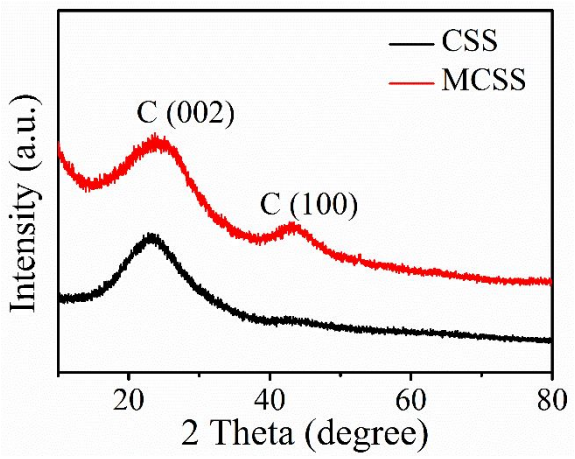

Figure S8. XRD patterns of CSS and MCSS.

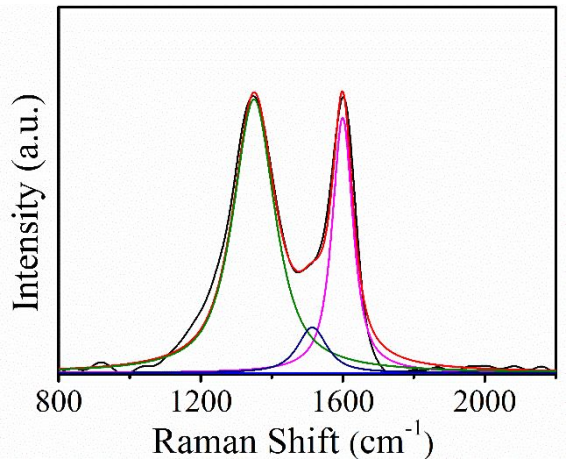

Figure S9. Raman spectra of MCSS.

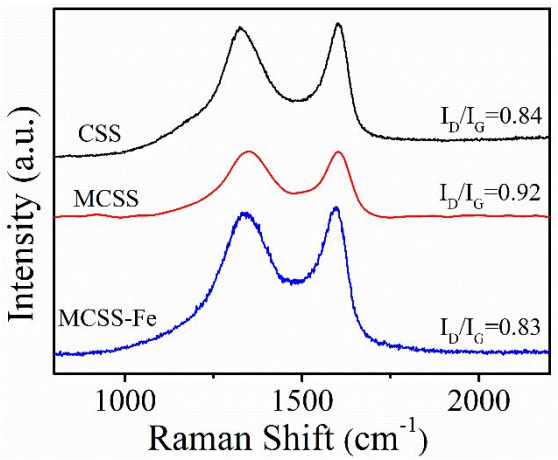

Figure S10. Raman spectra of MCSS.

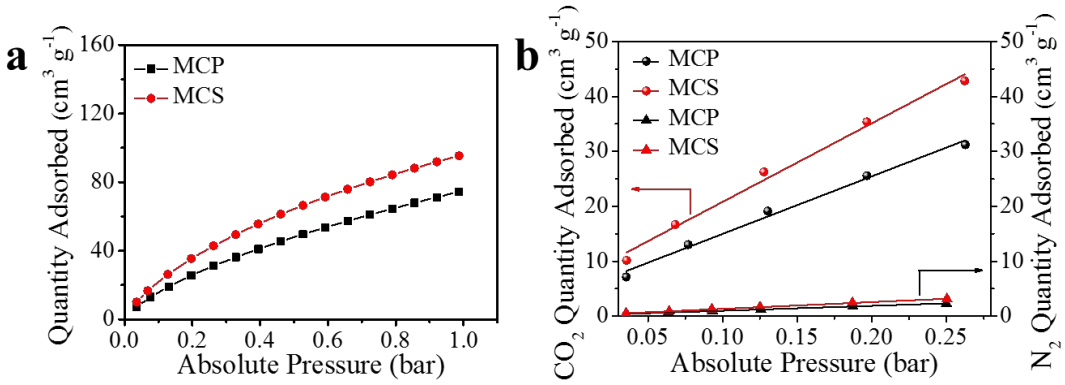

Figure S11. (a) CO_2 adsorption isotherms of MCP and MCS at 273 K, and (b) Initial N_2 and CO_2 uptake slopes of MCP and MCS used for selectivity calculations (CO_2 over N_2) in a pressure window of 0-0.26 bar.

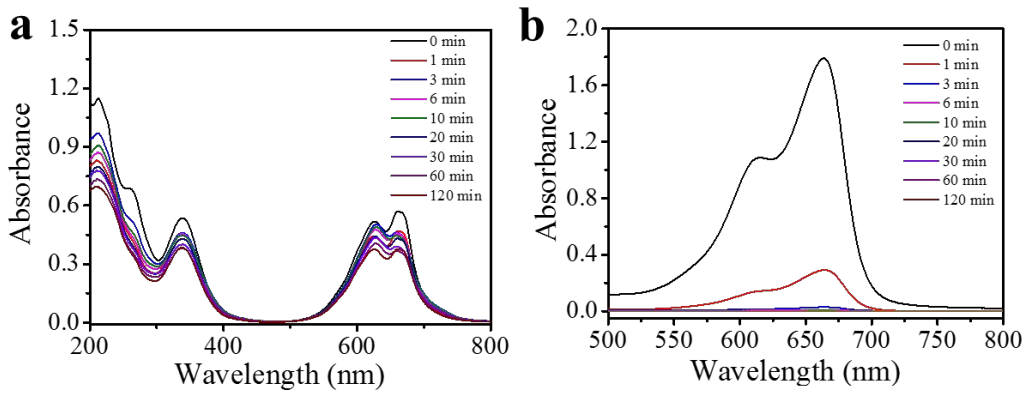

Figure S12. UV-Vis spectra of (a) RB21 and (b) MB for MCSS.

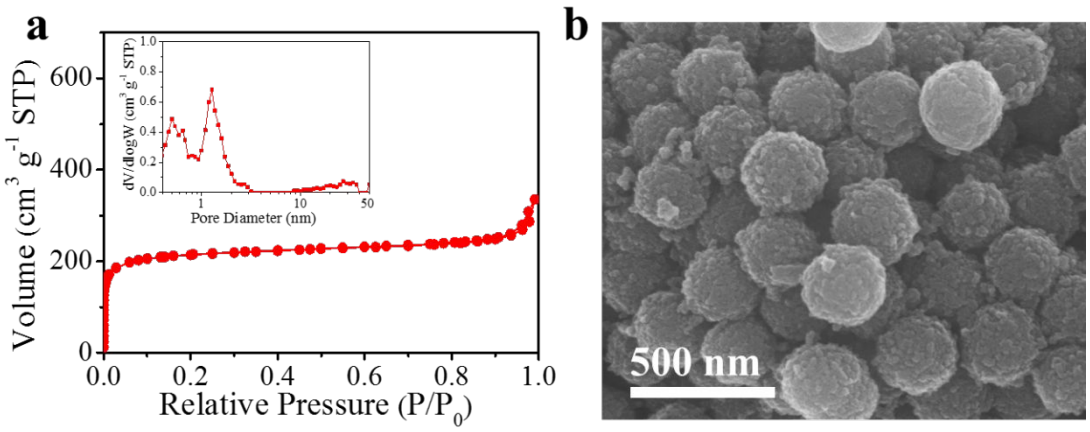

Figure S13. (a) N_2 adsorption-desorption isotherms and corresponding Pore size distribution of MCSS after adsorption of MB. (b) SEM image of MCSS after adsorption of MB.

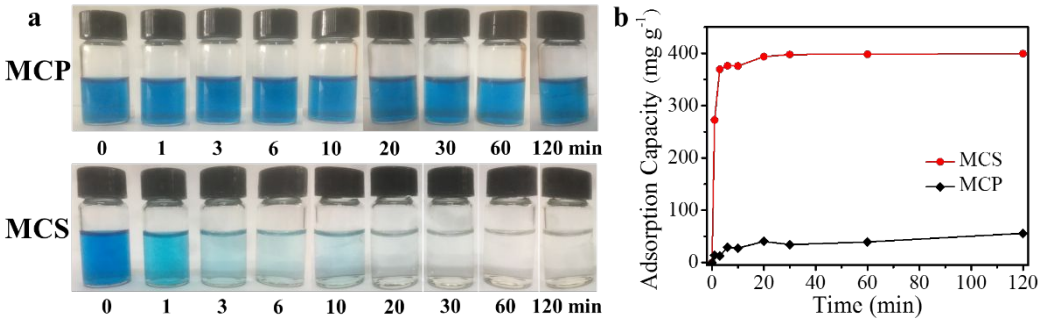

Figure S14. (a) Photograph of MB solutions with various times. (b) Time-dependent adsorption of MB by MCP and MCS.

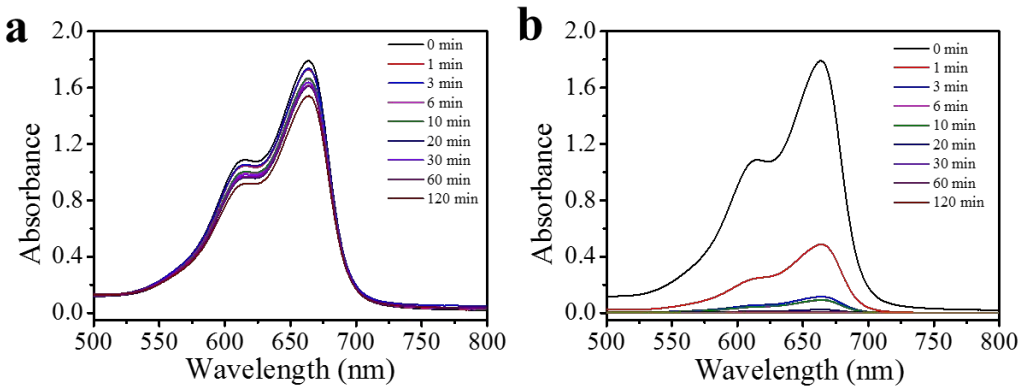

Figure S15. UV-Vis spectra of MB for (a) MCP and (b) MCS.

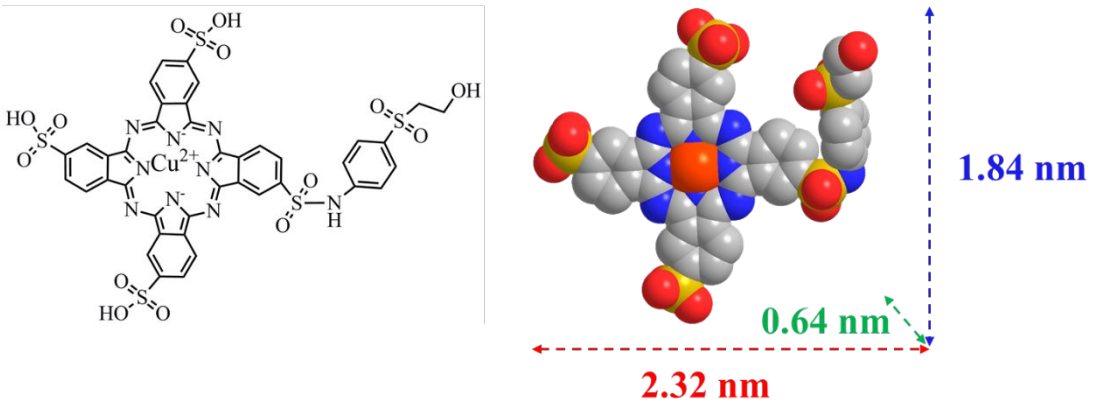

Figure S16. Molecule structure and 3D model of RB21. For 3D model, the H atoms are hidden for clarity.

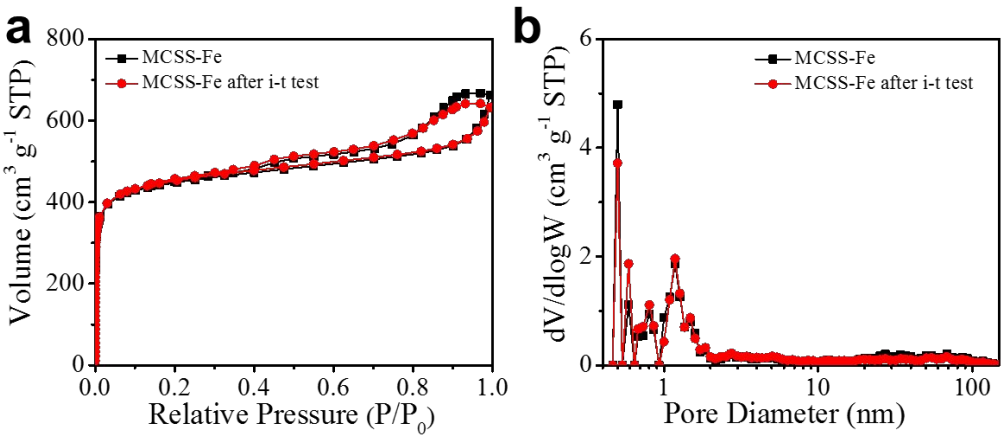

Figure S17. (a) N_2 adsorption-desorption isotherms of MCSS-Fe and MCSS-Fe after i-t test. (b) Pore size distribution of MCSS-Fe and MCSS-Fe after i-t test.

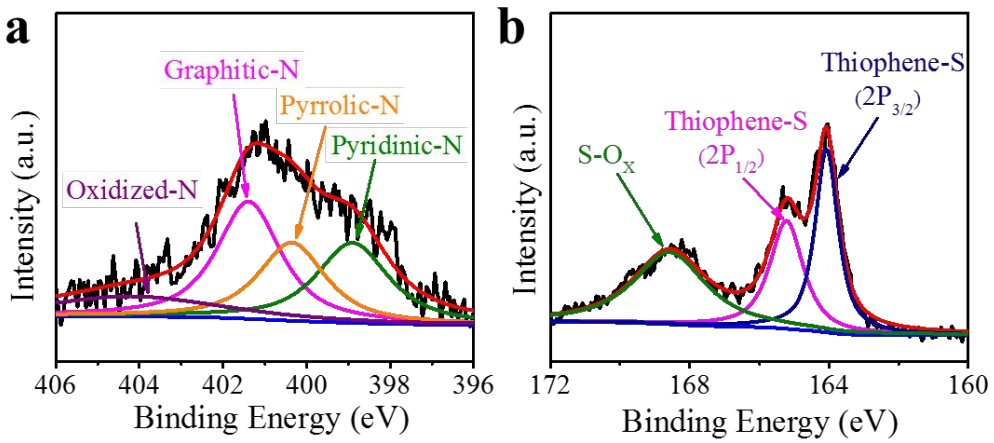

Figure S18. High resolution XPS spectra (a) N 1s and (b) S 2p of MCSS-Fe.

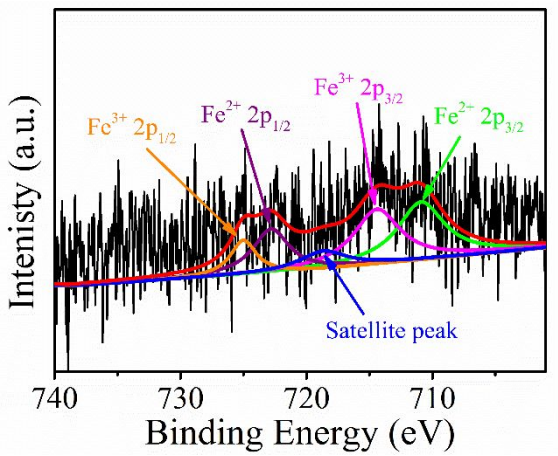

Figure S19. High resolution XPS spectra Fe 2p of MCSS-Fe.

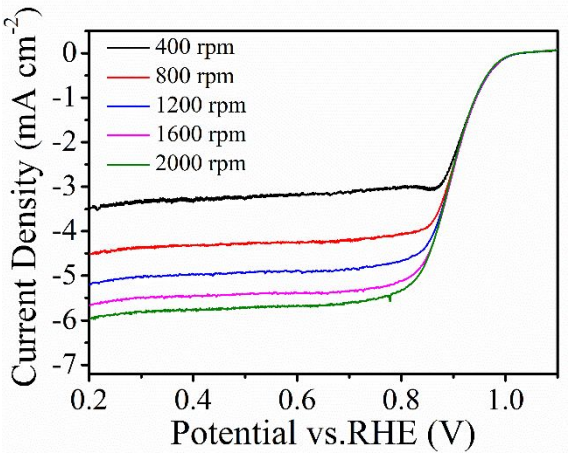

Figure S20. LSV curves of MCSS-Fe at different rotating speeds.

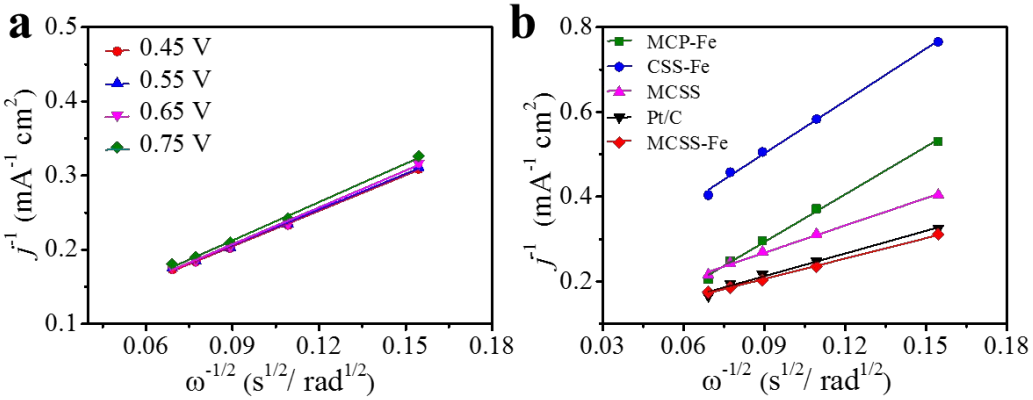

Figure S21. (a) Koutechy-Levich plots for MCSS-Fe and (b) Koutechy-Levich plots for MCP-Fe, CSS-Fe, MCSS, Pt/C and MCSS-Fe at 0.55 V.

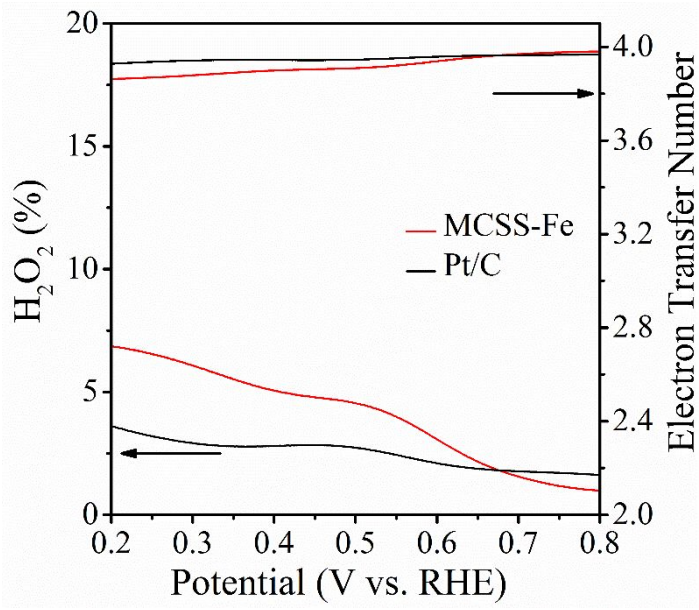

Figure S22. Peroxide yield and electron-transfer number of MCSS-Fe and Pt/C catalyst at various potentials based on the RRDE data.

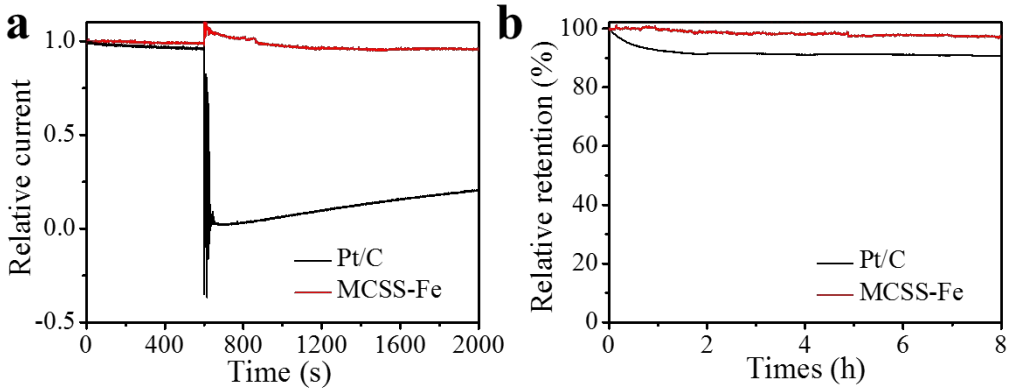

Figure S23. (a) Chronoamperometric curves of MCSS-Fe and Pt/C at 0.565 V followed by introducing methanol and (b) Chronoamperometric curves of MCSS-Fe and Pt/C at 0.57 V in O_2-saturated 0.1 M KOH at 600 rpm.

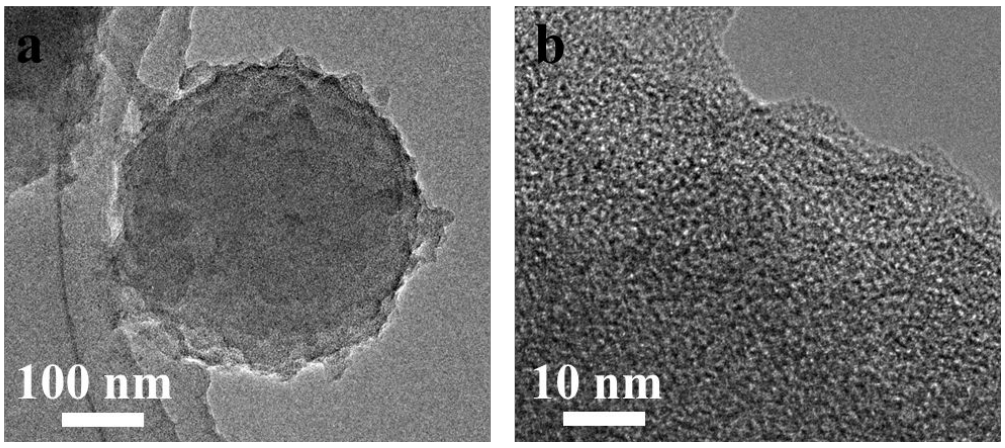

Figure S24. (a,b) HR-TEM images of MCSS-Fe after i-t test.

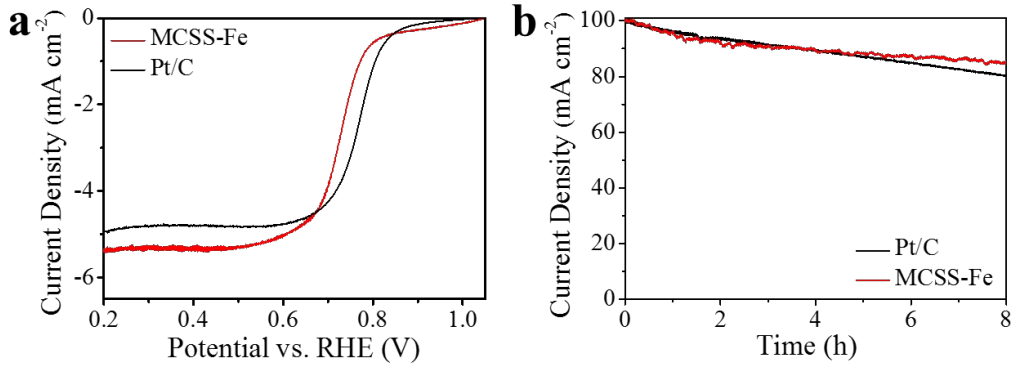

Figure S25. (a) ORR polarization curves of Pt/C, and MCSS-Fe samples in 0.5 M H_2SO_4 and (b) Chronoamperometric curves of MCSS-Fe and Pt/C at 0.4 V in O_2-saturated 0.5 M H_2SO_4 at 600 rpm.

Table S1. Element content of samples.

Samples	C content (at%)	N content (at%)	Si content (at%)	Fe content (at%)	S content (at%)	O content (at%)
CSS	36.63	1.11	18.86	0	0	43.40
MCSS	85.87	2.35	1.86	0	0	9.93
MCSS-Fe	85.07	2.84	2.04	0.37	2.04	8.38
MCP-Fe	91.30	2.91	0.72	0.2	0.71	4.17

Table S2. Comparison in the BET surface area and pore structure of MCSS and carbon spheres obtained through the silica templates.

Samples	S_{BET} (m^2 g^{-1})	Pore size (nm)	Silica template	Reference
MCSS	**2036**	**1.2**	**Nanosilica domain**	**This work**
O-MCS	1186	5.9	SiO_2	1
MCNs	1117	7	SiO_2	2
HMCNs	646	3.8	SiO_2	3
MC-MS-1	526	8.1	Silica inverse opal	4
N-HPCS	1137	2.5	SiO_2	5
HMCSs	771	2.1	SiO_2	6
egg-CMS	970	4	SiO_2	7
MCS	648	3	SiO_2	8
NHC	1538	3.2	SiO_2	9
HC-C18	1620	4.3	Organosilica	10
PHCSs	1520	1-25	SiO_2	11
P-N-CS	95	>7	SiO_2	12

Table S3. Comparison of ORR catalytic activity between MCSS-Fe and other Fe-based carbonous electrocatalysts in 0.1 M KOH solution.

Samples	Half-wave Potential (V vs.RHE)	References
MCSS-Fe	**0.89**	**This work**
FeP/Fe_2O_3@NPCA	0.81	13
Fe_{20}@N/HCSs	0.85	14
Ni-N_4/GHSs/Fe-N_4	0.83	15
CAN-Pc(Fe/Co)	0.85	16
Fe-N-C HNSs	0.87	17
Fe2-Z8-C	0.87	18
PFA-Fe10-900-ALP	0.86	19
S,N-Fe/N/C-CNT	0.85	20
Fe/SNC	0.86	21
Fe_1-HNC-500-850	0.84	22
Fe/NS/C-g-C_3N_4/TPTZ-1000	0.87	23
Fe-CNT/PC	0.88	24
Fe-SNC@900	0.83	25
p-Fe-N-CNFs	0.82	26

FeS/Fe_3C@N-S-C-800	0.87	27
OM-NCNF-FeN_x	0.84	28

Notes and references

(1) Du, J.; Liu, L.; Hu, Z.; Yu, Y.; Qin, Y.; Chen, A., Order Mesoporous Carbon Spheres with Precise Tunable Large Pore Size by Encapsulated Self–Activation Strategy. *Adv. Funct. Mater.* **2018,** *28*, 1802332.

(2) Wang, G.; Sun, Y.; Li, D.; Liang, H.–W.; Dong, R.; Feng, X.; Müllen, K., Controlled Synthesis of N–Doped Carbon Nanospheres with Tailored Mesopores through Self–Assembly of Colloidal Silica. *Angew. Chem. Int. Ed.* **2015,** *54*, 15191–15196.

(3) Chen, Y.; Xu, P.; Wu, M.; Meng, Q.; Chen, H.; Shu, Z.; Wang, J.; Zhang, L.; Li, Y.; Shi, J., Colloidal RBC–Shaped, Hydrophilic, and Hollow Mesoporous Carbon Nanocapsules for Highly Efficient Biomedical Engineering. *Adv. Mater.* **2014,** *26*, 4294–4301.

(4) Sun, Z.; Liu, Y.; Li, B.; Wei, J.; Wang, M.; Yue, Q.; Deng, Y.; Kaliaguine, S.; Zhao, D., General Synthesis of Discrete Mesoporous Carbon Microspheres through a Confined Self–Assembly Process in Inverse Opals. *ACS Nano* **2013,** *7*, 8706–8714.

(5) Pei, F.; An, T.; Zang, J.; Zhao, X.; Fang, X.; Zheng, M.; Dong, Q.; Zheng, N., From Hollow Carbon Spheres to N–Doped Hollow Porous Carbon Bowls: Rational Design of Hollow Carbon Host for Li–S Batteries. *Adv. Energy Mater.* **2016,** *6*, 1502539.

(6) Zhang, X.; Zhao, R.; Wu, Q.; Li, W.; Shen, C.; Ni, L.; Yan, H.; Diao, G.; Chen, M., Petal–like MoS_2 Nanosheets Space–Confined in Hollow Mesoporous Carbon Spheres for Enhanced Lithium Storage Performance. *ACS Nano* **2017,** *11*, 8429–8436.

(7) Wu, H.; Geng, J.; Ge, H.; Guo, Z.; Wang, Y.; Zheng, G., Egg–Derived Mesoporous Carbon Microspheres as Bifunctional Oxygen Evolution and Oxygen Reduction Electrocatalysts. *Adv. Energy Mater.* **2016,** *6*, 1600794.

(8) Jayaprakash, N.; Shen, J.; Moganty, S. S.; Corona, A.; Archer, L. A., Porous Hollow Carbon@Sulfur Composites for High–Power Lithium–Sulfur Batteries. *Angew. Chem. Int. Ed.* **2011,** *50*, 5904–5908.

(9) Zhou, W.; Xiao, X.; Cai, M.; Yang, L., Polydopamine–Coated, Nitrogen–Doped, Hollow Carbon–Sulfur Double–Layered Core–Shell Structure for Improving Lithium–Sulfur Batteries. *Nano Lett.* **2014,** *14*, 5250–5256.

(10) Valle–Vigón, P.; Sevilla, M.; Fuertes, A. B., Synthesis of Uniform Mesoporous Carbon Capsules by Carbonization of Organosilica Nanospheres. *Chem. Mater.* **2010,** *22*, 2526–2533.

(11) Zhang, K.; Zhao, Q.; Tao, Z. L.; Chen, J., Composite of sulfur impregnated in porous hollow carbon spheres as the cathode of Li–S batteries with high performance. *Nano Res.* **2013,** *6*, 38–46.

(12) Li, D.; Chen, H.; Liu, G.; Wei, M.; Ding, L.–x.; Wang, S.; Wang, H., Porous nitrogen doped carbon sphere as high performance anode of sodium–ion battery. *Carbon* **2015,** *94*, 888–894.

(13) Wu, K. Z.; Zhang, L.; Yuan, Y. F.; Zhong, L. X.; Chen, Z. X.; Chi, X.; Lu, H.; Chen, Z. H.; Zou, R.; Li, T. Z.; Jiang, C. Y.; Chen, Y. K.; Peng, X. W.; Lu, J., An Iron–Decorated Carbon Aerogel for Rechargeable Flow and Flexible Zn–Air Batteries. *Adv. Mater.* **2020,** *32*, 2002292.

(14) Wang, B.; Ye, Y.; Xu, L.; Quan, Y.; Wei, W.; Zhu, W.; Li, H.; Xia, J., Space‐Confined Yolk‐Shell Construction of Fe_3O_4 Nanoparticles Inside N‐Doped Hollow Mesoporous Carbon Spheres as Bifunctional Electrocatalysts for Long‐Term Rechargeable Zinc‐Air Batteries. *Adv. Funct. Mater.* **2020,** *30*, 2005834.

(15) Chen, J.; Li, H.; Fan, C.; Meng, Q.; Tang, Y.; Qiu, X.; Fu, G.; Ma, T., Dual Single–Atomic Ni–N4 and Fe–N4 Sites Constructing Janus Hollow Graphene for Selective Oxygen Electrocatalysis. *Adv. Mater.* **2020,** *32*, 2003134.

(16) Yang, S.; Yu, Y.; Dou, M.; Zhang, Z.; Dai, L.; Wang, F., Two–Dimensional Conjugated Aromatic Networks as High–Site–Density and Single–Atom Electrocatalysts for the Oxygen Reduction Reaction. *Angew. Chem. Int. Ed.* **2019,** *58*, 14724–14730.

(17) Chen, Y.; Li, Z.; Zhu, Y.; Sun, D.; Liu, X.; Xu, L.; Tang, Y., Atomic Fe Dispersed on N–Doped Carbon Hollow Nanospheres for High–Efficiency Electrocatalytic Oxygen Reduction. *Adv. Mater.* **2019,** *31*, 1806312.

(18) Liu, Q.; Liu, X.; Zheng, L.; Shui, J., The Solid–Phase Synthesis of an Fe–N–C Electrocatalyst for High–Power Proton–Exchange Membrane Fuel Cells. *Angew. Chem. Int. Ed.* **2018,** *57*, 1204–1208.

(19) Perez, L. C. P.; Sahraie, N. R.; Melke, J.; Elsaesser, P.; Teschner, D.; Huang, X.; Kraehnert, R.; White, R. J.; Enthaler, S.; Strasser, P.; Fischer, A., Polyformamidine–Derived Non–Noble Metal Electrocatalysts for Efficient Oxygen Reduction Reaction. *Adv. Funct. Mater.* **2018,** *28*.

(20) Pengzuo, C.; Tianpei, Z.; Lili, X.; Kun, X.; Yun, T.; Hui, X.; Lidong, Z.; Wensheng, Y.; Wangsheng, C.; Changzheng, W.; Yi, X., Atomically Dispersed Iron–Nitrogen Species as Electrocatalysts for Bifunctional Oxygen Evolution and Reduction Reactions. *Angew. Chem. Int. Ed.* **2017,** *56*, 610–614.

(21) Shen, H.; Gracia‐Espino, E.; Ma, J.; Zang, K.; Luo, J.; Wang, L.; Gao, S.; Mamat, X.; Hu, G.; Wagberg, T., Synergistic effects between atomically dispersed Fe−N− C and C− S− C for the oxygen reduction reaction in acidic media. *Angew. Chem. Int. Ed.* **2017,** *56*, 13800–13804.

(22) Zhang, X.; Zhang, S.; Yang, Y.; Wang, L.; Mu, Z.; Zhu, H.; Zhu, X.; Xing, H.; Xia, H.; Huang, B.; Li, J.; Guo, S.; Wang, E., A General Method for Transition Metal Single Atoms Anchored on Honeycomb–Like Nitrogen–Doped Carbon Nanosheets. *Adv. Mater.* **2020,** *32*, 1906905.

(23) Liu, X.; Chen, C.; Cheng, Q.; Zou, L.; Zou, Z.; Yang, H., Binary Nitrogen Precursor–Derived Porous Fe–N–S/C Catalyst for Efficient Oxygen Reduction Reaction in a Zn–Air Battery. *Catalysts* **2018,** *8*, 158.

(24) Sa, Y. J.; Seo, D.–J.; Woo, J.; Lim, J. T.; Cheon, J. Y.; Yang, S. Y.; Lee, J. M.; Kang, D.; Shin, T. J.; Shin, H. S.; Jeong, H. Y.; Kim, C. S.; Kim, M. G.; Kim, T.–Y.; Joo, S. H., A General Approach to Preferential Formation of Active Fe–Nx Sites in Fe–N/C Electrocatalysts for Efficient Oxygen Reduction Reaction. *J. Am. Chem. Soc.* **2016,** *138*, 15046–15056.

(25) Naveen, M. H.; Shim, K.; Hossain, M. S. A.; Kim, J. H.; Shim, Y. B., Template Free Preparation of Heteroatoms Doped Carbon Spheres with Trace Fe for Efficient Oxygen Reduction Reaction and Supercapacitor. *Adv. Energy Mater.* **2017,** *7*, 1602002.

(26) Hu, B. C.; Wu, Z. Y.; Chu, S. Q.; Zhu, H. W.; Liang, H. W.; Zhang, J.; Yu, S. H., SiO2–protected shell mediated templating synthesis of Fe–N–doped carbon nanofibers and their enhanced oxygen reduction reaction performance. *Energy Environ. Sci.* **2018,** *11*, 2208–2215.

(27) Kong, F.; Fan, X.; Kong, A.; Zhou, Z.; Zhang, X.; Shan, Y., Covalent Phenanthroline Framework Derived FeS@Fe_3C Composite Nanoparticles Embedding in N–S–Codoped Carbons as Highly Efficient Trifunctional Electrocatalysts. *Adv. Funct. Mater.* **2018,** *28*, 1803973.

(28) Cheng, C.; Li, S.; Xia, Y.; Ma, L.; Nie, C.; Roth, C.; Thomas, A.; Haag, R., Atomic Fe–Nx Coupled Open–Mesoporous Carbon Nanofibers for Efficient and Bioadaptable Oxygen Electrode in Mg–Air Batteries. *Adv. Mater.* **2018,** *30*, 1802669.